Calibration of Digital Amateur Cameras for Optical 3D Measurements With Element-Wise Weighted Total Least Squares (EW-WTLS) and Classical Least Squares: A Comparison

Sedat Doğan[1]

In order to improve the precision and accuracy of the calibration results, there are two general effects should be considered. One of them is the definition of the mathematical model of the calibration problem with respect to the physical nature of the problem, and the other one is the statistical model of the estimation of the calibration parameters. The estimation procedure is important for both dealing with the uncertainties of the observed measurements for computing the parameters and the numerical solution of the model. The classical least squares (LS) estimation model assumes that only the observation vector is erroneous while the data matrix is error free even its elements are the functions of the erroneous observations. These propagated errors in the data matrix elements stay as uncertainties in the classical LS model. The main purpose of this paper is to deal with those uncertainties in the camera calibration problem, by using the EW-WTLS estimation method and compare the results with the classical LS method. Both methods give almost the similar results. But at least in theory, the EW-WTLS estimation technique may be said to be more realistic than LS, by the means of its statistically more much realistic model.

Key words: *Camera Calibration, Bundle Adjustment, Computer Vision, Digital Photogrammetry, EW-WTLS, WTLS.*

1. Introduction

Accurate and precise camera calibration is one of the fundamental problems for precise measurements using images. Camera calibration procedure aims to find the intrinsic and extrinsic parameters of the camera. Since major concern of photogrammetry is with precise measurements using images, calibration of the image sensors has been and still is, of major concern [1]. One aspect of the camera calibration is to estimate the internal (intrinsic) parameters of the camera. These parameters determine how the image coordinates of a point is derived, given the spatial position of the point with respect to the camera [2]. Internal or intrinsic parameters of a camera are also referred as "internal orientation parameters" in photogrammetry community [3]. These internal parameters are necessary to define the position of the bundles of image points with respect to the camera and thus to define the image coordinates of the points which are projected onto the image plane by the bundles of light rays reflected from corresponding object points. The estimation of the geometrical relation between the camera and the scene, or between different cameras, is also an important aspect of calibration [2]. These external geometric relations are defined with the parameters so called external (or extrinsic) parameters. In photogrammetry, these external parameters are called as "external orientation parameters" [3]. The accuracy and the precision of the calibration parameters directly affect the accuracy and the precision of 3D measurements from images.

In order to improve the accuracy of the calibration parameters, two general effects should be considered. One of them is the definition of the parameters with respect to their physical natures, namely the mathematical model of the camera, and the second one is the estimation procedure of the parameters of the defined model within a statistically optimal way based on the nature of the errors of the input data. While the first group of the effects, i.e. the definition of the parameters and the relations between them, is important to represent the camera model as close as to physical reality; the second group's effects, i.e. the estimation procedure is important for both dealing with the uncertainties of the measurements performed for computing the parameters, and the numerical solution of the model.

In general, the mathematical model of the camera calibration problem is defined by either a linear bundle model or by a nonlinear bundle model which of two are both based on the ideal pinhole camera model. Linear models are usually preferred by the computer vision community, since linear models do not require initial approximations for the parameters, and thus more appropriate for the computer vision tasks. On the other side, the photogrammetry community prefers the non-linear bundle adjustment technique, which defines the imaging geometry with nonlinear co-linearity equations of corresponding object and image points. However, this non-linear model requires initial approximations of the unknown parameters. Initial approximations are computed from either linear models such as direct linear transformation (DLT) or any other closed form analytical solutions of the perspective projection. After the initial approximations of the parameters have been found, an iterative estimation algorithm is performed to find the final optimized values of the parameters. Bundle

[1] *Sedat Doğan,* Department of Geomatics Engineering, Engineering Faculty, Ondokuz Mayis University, 55200 Samsun, Turkey; sedatdo@omu.edu.tr

adjustment algorithm performed in such a way is very flexible and much more precise method than others for 3D photogrammetric measurement and reconstruction tasks from stereo images. Here the flexibility of the model means that any satisfactory number of intrinsic parameters representing the lens distortions and some other systematic error types may be inserted into the bundle adjustment model. Furthermore, tie points can also be used to improve the redundancy of the model.

This paper gives the solution of the camera calibration problem with the nonlinear bundle adjustment approach, and uses the EW-WTLS estimation technique for the calibration parameters. Before estimation procedure, variances of the all data are computed and then proper weighting matrices for each of the independent rows of the data matrix are found. The error free columns and any other error free elements of the data matrix are not modified (or corrected). And thus the EW-WTLS estimation method models the calibration problem more realistically by the means of the statistical model of the errors. This advanced theoretical basis of the EW-WTLS model generally causes someone to expect more precise and accurate results from EW-WTLS than LS. But as will be seen in the later sections of the paper, this kind of expectations are not necessary since both methods are derived from the almost same roots, as argued by [4]. For a detailed reading of the various estimation models originated from the least squares estimation approach, the reader may refer to [5]. Furthermore, it will also be seen that the estimation results of EW-WTLS and LS are almost the same by the means of precision and accuracy computed from the check point coordinates. But however, even two methods give similar precisions, there are slight differences between EW-WTLS and LS estimated parameter values. These differences mainly arise from the difference of the underlying statistical models. Thus it may be said that at least from the theoretical point of view, the EW-WTLS results with their slight differences from LS, must be more realistic and so these results may be preferred as the final values of the parameters. But notice that the more realism of the statistical model does not mean better precision and accuracy. In the next section, an overview of the state of the art of the various total least squares (TLS) models and camera calibration problem in the literature is given.

1.1 TLS Methods and Camera Calibration: The State of the Art

The TLS method was firstly introduced by Golub and Van Loan [6]. This TLS technique solves an over-determined system of equations of the form $\boldsymbol{Ax} \approx \boldsymbol{B}$, where $\boldsymbol{A} \in \boldsymbol{\mathcal{R}}^{m\times n}$, $\boldsymbol{B} \in \boldsymbol{\mathcal{R}}^{m\times d}$ are given data and $\boldsymbol{x} \in \boldsymbol{\mathcal{R}}^{n\times d}$ is unknown parameter vector/matrix. Here m is the number of the equations and n × d is the number of unknowns. If m > n, there is no exact solution for x, so an approximate solution with an optimization prob lem is searched [6-8]. TLS is essentially a generalization of the least squares (LS) method by assuming that the data both in $\boldsymbol{A}$ and $\boldsymbol{B}$ are perturbed, i.e. erroneous. In the classical LS, only the data in $\boldsymbol{B}$ are assumed to be perturbed and its optimization model is given by equation (1).

$$\{\hat{\boldsymbol{x}}_{ls}, \Delta\boldsymbol{B}_{\boldsymbol{ls}}\} = \underset{\boldsymbol{x},\Delta\boldsymbol{B}}{arg\,min} \|\Delta\boldsymbol{B}\|_F \; subject\ to\ \boldsymbol{Ax} = \boldsymbol{B} + \Delta\boldsymbol{B} \tag{1}$$

In the above equation, the optimization criterion is defined so that it corrects the data **B** as little as possible in the sense of Frobenius norm. The corrected system of equations $\mathbf{Ax} = \widehat{\mathbf{B}}, \widehat{\mathbf{B}} = \mathbf{B} + \Delta\mathbf{B}$ has exact solution [8]. When considering the real problems, the data matrix **A** has also data elements which are either directly the measurements themselves or the functions of the measurements. Then intuitively it is clear that the data matrix **A** is also perturbed by the random measurement errors. This real case is the TLS case. TLS model searches for the minimal corrections $\Delta\mathbf{A}$ and $\Delta\mathbf{B}$ on the given data **A** and **B**. Then the corrected system is obtained as $\widehat{\mathbf{A}}\mathbf{x} = \widehat{\mathbf{B}}$, $\widehat{\mathbf{A}} = \mathbf{A} + \Delta\mathbf{A}$ and $\widehat{\mathbf{B}} = \mathbf{B} + \Delta\mathbf{B}$ and now it has unique solution with the optimization criterion given by the Frobenius norm as follows: [8].

$$\{\hat{\boldsymbol{x}}_{tls}, \Delta\boldsymbol{A}_{tls}, \Delta\boldsymbol{B}_{tls}\} = \underset{\boldsymbol{x},\Delta\boldsymbol{A},\Delta\boldsymbol{B}}{arg\,min} \|\Delta\boldsymbol{A};\ \Delta\boldsymbol{B}\|_F \; subject\ to\ (\boldsymbol{A} + \Delta\boldsymbol{A})\boldsymbol{x} = \boldsymbol{B} + \Delta\boldsymbol{B} \tag{2}$$

is obtained, and $\hat{\mathbf{x}}_{\mathrm{tls}}$ is the estimated parameter vector.

In order to solve the TLS optimization problem given by equation (2), some reasonable assumptions are required about the unknown corrections (or perturbations) $\Delta\mathbf{A}$ and $\Delta\mathbf{B}$ respectively. The differences between various TLS models and their solution approach mainly arise from the assumptions made on the nature of the data perturbations. Since the perturbations can be considered as errors deviating the data matrices from their unknown true values say $\mathbf{A_0}$ and $\mathbf{B_0}$, the assumptions are constructed on the distribution of the errors in a proper manner.

The basic TLS problem introduced by Golub and Van Loan in [6] assumes that the errors are randomly distributed by zero mean and with a covariance matrix which is multiple of the identity matrix. Under this assumption, the basic TLS assumes that all elements of **A** and **B** are perturbed and so it modifies the elements to make corrections. Robust and efficient methods exist for the solution of this simplest case of TLS based

on the singular value decomposition (SVD). In this simple form, the TLS solution is given analytically in terms of the d smallest right singular vectors of the augmented data matrix $\mathbf{D} = [\mathbf{A}\ \mathbf{B}]$ [6-10].

In the most of the real problems, the errors in the data matrix **D** are not identical and not have common variances. For example, in linear regression models, one column of **D** which corresponds to intercept parameter is constant, namely error free. In similar way, in the camera calibration model of the bundle adjustment problem, two columns of the data **D** are constants namely, known exactly and so error-free. In such general cases, the fixed columns should not be modified. Since the variances of the fixed columns are zero, they have no error distribution function. In this case, a more general TLS model is used not to modify the fixed columns. These constant columns of **D** are linearly dependent to others and so a rank reduction process should be performed to find an exact solution. This rank reduction problem may be thought as a subspace approximation problem [11-13]. If the rest of the erroneous columns of **D** have an iid error distribution with a common variance, then this is called mixed LS-TLS problem [7].

It is clear that the error distribution assumption is the same as the basic TLS for the erroneous columns of the mixed LS-TLS. In order to deal with the fixed columns of **D**, there are various solution proposals in the literature such as [5, 7, 14, 15]. Another proposal on more general constrained subspace perturbations has been given by [16]. If the error distribution model of the mixed LS-TLS is generalized to the case of correlated errors for the erroneous columns, then this more general case is called generalized TLS (GTLS). i.e., the data matrix has one or more fixed columns and its perturbed (non-fixed) columns have an error distribution with a common covariance matrix. Solution of the GTLS is given in detail in [7]. A detailed comparison of GTLS and LS is given in [17]. This paper gives also the use of the GTLS in computer vision. However the GTLS still has a problem for some real applications. Because the GTLS assumes a column is fixed only if the all elements of that column are constant. Otherwise, the rest of the elements outside the fixed columns are assumed perturbed, even some of them are really constants. For example assume that the data matrix **D** has two exactly fixed columns and three perturbed columns. Let some of the elements of the three perturbed columns be constant while the others are perturbed. In this case the GTLS modifies those constant elements too as if they were perturbed. Then this situation is not realistic and in this case the error distribution is not identical anymore. The GTLS model assumes that the errors of **D** are row-wise independent and correlated within the rows with identical covariance matrix [7, 10]. This GTLS still does not capture the errors which are row-wise independent and have non-identical covariance matrices within a row.

Further generalization of the GTLS to capture the case when the elements of **D** are independent but not identically distributed with different error covariances is proposed in [18] and it is called weighted total least squares (WTLS). There are various proposed algorithms for the solution of WTLS problems. We refer the reader to [19] for reading the extensive overview of TLS methods, their historical progressions and various parameter representations, as well as WTLS. WTLS can solve the most general cases of the TLS with various approaches by using effective solution proposals presented in the literature [8, 10, 19-22]. In the geodesy literature, there are also various proposals for the solution of the TLS models such as [4, 5, 23, 24]. There are also very interesting discussions on the comparison of TLS and classical LS techniques in the geodesy literature [4, 25]. These last two papers asserts that it is unnecessary task to compare the TLS and LS methods, since they are both based on standard LS approach.

In this paper, element-wise weighted TLS (EW-WTLS) method was used to solve the camera calibration problem. The reason for using the EW-WTLS is that the camera calibration problem mostly fits to this model. The EW-WTLS assumes that the rows of the data matrix **D** are independent from each other and each element in any row may have different variance than others as well as zero variance if it is constant namely, error-free. The elements of the same row may also have column-wise correlations with each other. In the case of the camera calibration problem, the rows of the data matrix **D** correspond to measurements and their some functional values. The measurements are independent from each other and so are the rows of the data matrix. Each row has its own covariance matrix, which represent the variance-covariance information between this row's elements. In the present paper, the covariance matrices of the each row of the data matrix are diagonal matrices, implying that there are no correlations between the elements of the same row. Because, there no reason found to assume that those elements are correlated since those elements are functions of the independent observations. Before the estimation procedure, proper weight matrices for each row are computed from their covariance matrices. The details are given in section 3.

TLS models for camera calibration problems have been studied and discussed in the literature of the computer vision community but all of them have used the linear homography or linear bundle models for the mathematical model of the camera calibration. But however, still there is not any solution performed with the EW-WTLS method [12, 13, 17]. There are no TLS or EW-WTLS studies by using nonlinear bundle adjustment model in computer vision community. On the other side, there are only two studies that use the TLS methods in photogrammetry. One of them gives space resection (also called triangulation) solution with basic TLS and assumes that intrinsic parameters are known [26]. Since the intrinsic parameters are assumed

to be known in this study, it is not a camera calibration problem. The other TLS study in photogrammetry has been used for image registration problem [27].

2. Mathematical Models of Self Calibration and TLS Estimation

2.1 Self Calibration Model

The calibration model of self calibration with bundle adjustment is based on the co-linearity equations derived from the ideal pinhole camera model. The main problem is to define the systematic error sources which cause the physical realization of the model to deviate from its ideal case. The mathematical model of the well known co-linearity equations is as follows:

$$\xi = \xi_0 - c\,\frac{r_{11}(X-X_0)+r_{21}(Y-Y_0)+r_{31}(Z-Z_0)}{r_{13}(X-X_0)+r_{23}(Y-Y_0)+r_{33}(Z-Z_0)} \tag{3.a}$$

$$\eta = \eta_0 - c\,\frac{r_{12}(X-X_0)+r_{22}(Y-Y_0)+r_{32}(Z-Z_0)}{r_{13}(X-X_0)+r_{23}(Y-Y_0)+r_{33}(Z-Z_0)} \tag{3.b}$$

where ξ, η are the image coordinates of an object point P, ξ_0, η_0 are the image coordinates of the principal point, c is the camera constant and approximately equal to the focal length and X, Y, Z are the object coordinates of the object point P. X_0, Y_0, Z_0 are the object coordinates of the projection center of the camera and these are different for each of the images together with the r_{ik} parameters. Here r_{ik} are the elements of the orthonormal rotation matrix **R** of the corresponding image with $\mathbf{R} \in \boldsymbol{\mathcal{R}}^{3\times3}$. The r_{ik} entries of the rotation matrix **R** are some trigonometric functions of three rotation angles ω, φ, κ which are the rotations of the camera coordinate system with respect to the object coordinate system and are they the successive rotations about the X, Y and Z axes respectively. Instead of these axial rotations, one could use Euler angles or quaternions as well.

In equations (3.a) and (3.b), ξ_0, η_0 and c are the intrinsic parameters of the camera (or of the images taken with it). $X_0, Y_0, Z_0, \omega, \varphi, \kappa$ are the extrinsic parameters. The orthonormal rotation matrix is a proper rotation matrix. In this paper, the following rotation matrix has been used.

$$\mathbf{R} = \begin{bmatrix} \cos\varphi.\cos\kappa & -\cos\varphi.\sin\kappa & \sin\varphi \\ \cos\omega.\sin\kappa + \sin\omega.\sin\varphi.\cos\kappa & \cos\omega.\cos\kappa - \sin\omega.\sin\varphi.\sin\kappa & -\sin\omega.\cos\varphi \\ \sin\omega.\sin\kappa - \cos\omega.\sin\varphi.\cos\kappa & \sin\omega.\cos\kappa + \cos\omega.\sin\varphi.\sin\kappa & \cos\omega.\cos\varphi \end{bmatrix} \tag{4}$$

The co-linearity equations given by the equations (3) represent the ideal pinhole camera model. However, this ideal model differs from the ideal case due to the distortion effects of the optical system of a real physical camera. In addition to the lens distortions, the sensor system may also lead to distortions in some degree. Lens distortions of the real cameras cause the light rays (in other words projection rays) to change their linear paths before reaching to the sensor plane (projection plane/image plane). Deviation of any light ray from its ideal path results in some changes of the image coordinates of the point it projects on to the image plane. For accurate and precise measurements, the deviations from the ideal case should be computed and the image coordinates should be corrected by eliminating those changes properly. Let $\Delta\xi$ and $\Delta\eta$ be the corrections of the distortion effects for image coordinates ξ and η of an image point respectively. Then the equations (3) can be re-written as follows:

$$f_x = (\xi - \xi_0) = -c\,\frac{Z_x}{N} + \Delta\xi \tag{5.a}$$

$$f_y = (\eta - \eta_0) = -c\,\frac{Z_y}{N} + \Delta\eta \tag{5.b}$$

where, Z_x and Z_y are the numerators of the equations (3.a) and (3.b) respectively and N is the denominators of those equations. In equations (5), ξ and η coordinates of an image point are corrected by the corrections $\Delta\xi$ and $\Delta\eta$. Here, $\Delta\xi$ and $\Delta\eta$ are assumed to be resulted from the additive systematic effects of the lenses and the sensor system. To model the systematic effects, namely the systematic errors, there are various proposals in the literature such as [1, 28-30].

The main and the most important systematic error sources are radial distortion and eccentricity of the lenses. Furthermore there are affine effects arise from the improper mounting of the optical system relative to the sensor plane. In the proper case, the lenses must be parallel to the sensor plane otherwise, projective distortions occur on the scanned image. Advanced digital cameras such as SLR and DSLR, almost satisfy this condition so, for them these effects can be defined with two affine parameters. But however, cheaper digital cameras may have a considerable projective distortion so for them more parameters can be used to model these mentioned effects [30]. According to the brief explanations above, the corrections of the image coordinates may be expressed as follows: [31].

$$\Delta\xi = \Delta\xi_{radi.} + \Delta\xi_{ecc.} + \Delta\xi_{aff.} \tag{6.a}$$

$$\Delta\eta = \Delta\eta_{radi.} + \Delta\eta_{ecc.} + \Delta\eta_{aff.} \tag{6.b}$$

where, the subscripts "radi.", "ecc." and "aff." denote the intrinsic parameters those are radial lens distortion, eccentricity distortion and the affinity effects respectively. Since ξ_0, η_0, c are captured directly at the end of the estimation process, their changes are numerically zero in equations (6) and so they are omitted in the above equations. Brown defines in [28] 29 parameters for the systematic errors but 10 of them are suggested for the digital cameras as follows:

With the abbreviation $r^2 = \bar{\xi}^2 + \bar{\eta}^2$ where $\bar{\xi} = \xi - \xi_0,\ \bar{\eta} = \eta - \eta_0$;

$$\Delta\xi_{radi.} = \bar{\xi}[k_1 r^2 + k_2 r^4 + k_3 r^6] \tag{7.a}$$

$$\Delta\eta_{radi.} = \bar{\eta}[k_1 r^2 + k_2 r^4 + k_3 r^6] \tag{7.b}$$

where kj (j=1, 2, 3) are the radial distortion coefficients.

$$\Delta\xi_{ecc.} = \left(r^2 + 2\bar{\xi}^2\right)P_1 + 2\bar{\xi}\bar{\eta}P_2 \tag{8.a}$$

$$\Delta\eta_{ecc.} = 2\bar{\xi}\bar{\eta}P_1 + (r^2 + 2\bar{\eta}^2)P_2 \tag{8.b}$$

where, P1 and P2 are the eccentricity coefficients, and

$$\Delta\xi_{aff.} = -b_1\bar{\xi} + b_2\bar{\eta} \tag{9.a}$$

$$\Delta\eta_{aff.} = b_2\bar{\xi} \tag{9.b}$$

where, b_1 is affine scale and b_2 is the non-orthogonality effect of the image coordinate axes. Here both these two parameters are referred as affine parameters. The reader is referred to [1, 3, 28, 30, 31] etc. for the derivation of the above equations. The complete set of corrections as a whole is written as follows:

$$\Delta\xi = \bar{\xi}k_1 r^2 + \bar{\xi}k_2 r^4 + \bar{\xi}k_3 r^6 + \left(r^2 + 2\bar{\xi}^2\right)P_1 + 2\bar{\xi}\bar{\eta}P_2 - b_1\bar{\xi} + b_2\bar{\eta} \tag{10.a}$$

$$\Delta\eta = \bar{\eta}k_1 r^2 + \bar{\eta}k_2 r^4 + \bar{\eta}k_3 r^6 + 2\bar{\xi}\bar{\eta}P_1 + (r^2 + 2\bar{\eta}^2)P_2 + b_2\bar{\xi} \tag{10.b}$$

If the systematic corrections $\Delta\xi$ and $\Delta\eta$ are substituted in equations (5), the general non-linear camera calibration equations are obtained. This general calibration model contains ten intrinsic parameters and for each image six extrinsic parameters. If there are s images taken for calibration from the same camera, then the total number of unknown calibration parameters is (10 + 6 × s), because the ten intrinsic parameters are the same for all images since they were taken with the same camera. On the other side, each image has its own six extrinsic parameters which represent the orientation of each image's camera coordinate system with respect to the object coordinate system. These external parameters are the rotation angles ω_i, φ_i and κ_i between each camera position and the object coordinate system. Rest of the three parameters X_{0i}, Y_{0i}, Z_{0i} are the object coordinates of the projection center of the image i with i=1,2,…,s.

This general calibration model may also be augmented by using tie-points, which are the points seen at least in two images and their object coordinates are unknown. These tie points are useful especially to strengthen the relative orientation of images by the means of their co-linear lines must intersect in the object space and cited on the epipolar plane. This intersection constraint implicitly improves the power of the relative orientation of the images. Although one tie point brings three unknowns which are its object coordinates, it increases the redundancy of the model since a tie point provides at least four observation equations. Then if a tie point is seen in three images, then since there are six image coordinates of that point are measured, this tie point brings three unknowns and six observation equations. If the number of tie points used for calibration is t, then the total number of unknowns of the model becomes (10 + 6 × s + 3 × t).

Equations (5) are nonlinear in terms of the unknown calibration parameters. Before the optimization procedure, these equations should be linearized. Taylor series expansion may be used for the linearization about the approximate values of the unknowns. Then an iterative solution of the optimization problem is applied until some predefined stopping criterions are met. Linearized equations are in the following form:

$$\begin{aligned} f_x = (\xi - \xi_0) = f_x\left(c^0, \xi_0^0, \eta_0^0, b_1^0, b_2^0, k_1^0, k_2^0, k_3^0, P_1^0, P_2^0, X_{0i}^0, Y_{0i}^0, Z_{0i}^0, \omega_i^0, \varphi_i^0, \kappa_i^0, X_{tie_j}^0, Y_{tie_j}^0, Z_{tie_j}^0\right) + \\ \frac{\partial f_x}{\partial c}dc + \frac{\partial f_x}{\partial \xi_0}d\xi_0 + \cdots + \frac{\partial f_x}{\partial P_1}dP_1 + \frac{\partial f_x}{\partial P_2}dP_2 + \cdots + \frac{\partial f_x}{\partial Z_0}dZ_0 + \frac{\partial f_x}{\partial \omega_i}d\omega_i + \cdots + \frac{\partial f_x}{\partial \kappa_i}d\kappa_i + \frac{\partial f_x}{\partial X_{tie\_j}}dX_{tie\_j} + \cdots + \\ \frac{\partial f_x}{\partial Z_{tie\_j}}dZ_{tie\_j} + \text{higher order terms} \end{aligned} \tag{11}$$

f_y is linearized by the same way as equation (11). Higher order terms are ignored. Here, superscript zeros represent the initial approximate values of the unknowns, i =1, 2,…,s and s is the number of the images used for calibration. Furthermore, j=1,...t is the index of the corresponding tie points. The partial derivatives are given explicitly in [3]. Let **x** be the unknown parameter vector as follows:

$$\mathbf{x} = \left[dc\ d\xi_0\ d\eta_0\ db_1\ db_2\ dk_1\ dk_2\ dk_3\ dP_1\ dP_2\ dX_{0i}\ dY_{0i}\ dZ_{0i}\ d\omega_i\ d\varphi_i\ d\kappa_i\ dX_{tie\_j}\ dY_{tie\_j}\ dZ_{tie\_j}\right]^T \tag{12}$$

where, $X_{tie\_j}, Y_{tie\_j}, Z_{tie\_j}$ are unknown tie points ' coordinates. In this paper 16 tie points were used for calibration. The linearized equations are written in the matrix form as below:

$$\begin{bmatrix} \frac{\partial f_x}{\partial c} & \frac{\partial f_x}{\partial \xi_0} & \cdots & \frac{\partial f_x}{\partial X_{0i}} & \frac{\partial f_x}{\partial Y_{0i}} & \frac{\partial f_x}{\partial Z_{0i}} & \frac{\partial f_x}{\partial \omega_i} & \frac{\partial f_x}{\partial \varphi_i} & \frac{\partial f_x}{\partial \kappa_i} & \cdots & \frac{\partial f_x}{\partial \omega_s} & \frac{\partial f_x}{\partial \varphi_s} & \frac{\partial f_x}{\partial \kappa_s} & \frac{\partial f_x}{\partial X_{tie_j}} & \frac{\partial f_x}{\partial Y_{tie_j}} & \frac{\partial f_x}{\partial Z_{tie_j}} & \cdots \\ \frac{\partial f_y}{\partial c} & \frac{\partial f_y}{\partial \xi_0} & \cdots & \frac{\partial f_y}{\partial X_{0i}} & \frac{\partial f_y}{\partial Y_{0i}} & \frac{\partial f_y}{\partial Z_{0i}} & \frac{\partial f_y}{\partial \omega_i} & \frac{\partial f_y}{\partial \varphi_i} & \frac{\partial f_y}{\partial \kappa_i} & \cdots & \frac{\partial f_y}{\partial \omega_s} & \frac{\partial f_y}{\partial \varphi_s} & \frac{\partial f_y}{\partial \kappa_s} & \frac{\partial f_y}{\partial X_{tie_j}} & \frac{\partial f_y}{\partial Y_{tie_j}} & \frac{\partial f_y}{\partial Z_{tie_j}} & \cdots \\ \vdots & \vdots & \vdots & \vdots & \vdots & \vdots & \vdots & \vdots & \vdots & \vdots & \vdots & \vdots & \vdots & \vdots & \vdots & \vdots & \vdots \end{bmatrix} \begin{bmatrix} dc \\ \vdots \\ d\kappa_s \\ \vdots \\ dZ_{tie_j} \end{bmatrix} = \begin{bmatrix} l_1 \\ l_2 \\ \vdots \end{bmatrix} \tag{13}$$

Let **A** denote the first matrix, **x** denote the second term vector and **b** denote the right hand vector. Then equations (13) are in the linear form of $\mathbf{Ax} = \mathbf{b}$. Above equations are only for one control point or tie point in *s* images. If equations (13) are written for a control point then the partial derivatives with respect to the tie point coordinates are zero. The matrix **A** and the vector **b** should be augmented for all control and tie points. The calibration experiment given in section 3, contains 52 control points and 16 tie points. According to their visibility status in each image, the dimensions of the matrix and vectors of the experiment are $\mathbf{A} \in \boldsymbol{\mathcal{R}}^{(532)\times(82)}$, $\mathbf{x} \in \boldsymbol{\mathcal{R}}^{(82)\times 1}$, and $\mathbf{b} \in \boldsymbol{\mathcal{R}}^{(532)\times 1}$. Now the linearized calibration equations of the form $\mathbf{Ax} = \mathbf{b}$ are ready to be optimized with the EW-WTLS estimation method.

2.2 Mathematical Model and Solution of EW-WTLS

This paper uses the EW-WTLS model based on the solution given by [8-10, 19] for camera calibration. In this section, the main concepts and the tricks of the model are briefly explained and the interested readers are referred to papers given above for the detailed analysis of the EW-WTLS method.

The EW-WTLS method corrects the data matrix $\mathbf{D} = [\mathbf{A}\ \mathbf{B}]$ by applying the corrections $\Delta\mathbf{D}$ that makes the system $(\mathbf{A} + \Delta\mathbf{A})\mathbf{x} = \mathbf{B} + \Delta\mathbf{B}$ solvable. The cost function of the estimation procedure is a weighted Frobenius norm of the corrections. Each row of $\Delta\mathbf{D}$ is independent from the others and has its own covariance matrix which represents the variances of the corresponding elements of the each row and the covariances between these row elements if exist. If the elements within a row are independent from each other, then their covariances are zero and the covariance matrix of that row is diagonal and the diagonal elements represent the variances of the elements of that row. If the variances of some diagonal elements are zero then the covariance matrix is singular. EW-WTLS solves this singular problem too. The covariance matrices are square and their dimensions are defined with the number of the elements of the rows and this is equal to the number of the columns of the data matrix **D**. Let $\Delta\mathbf{d}_i^T$ be the ith row of $\Delta\mathbf{D}$, i.e., $\Delta\mathbf{D}^T = [\Delta\mathbf{d}_1 \ \ldots \ \Delta\mathbf{d}_m]$. The EW-WTLS cost function is $\sum_{i=1}^{m} \left\| \mathbf{V}_{di}^{-1/2} \Delta\mathbf{d}_i \right\|_2^2$ [8, 19]. Here, $\mathbf{V}_{di}$ is the covariance matrix of the row $\mathbf{d}_i$ of $\Delta\mathbf{D}$, and is of the form as in follows:

$$\mathbf{V}_{di} = \begin{bmatrix} var(e_1e_1) & cov(e_1e_2) & \ldots & cov(e_1e_n) & cov(e_1e_{n+1}) & \ldots & cov(e_1e_{n+d}) \\ cov(e_2e_1) & var(e_2e_2) & \ldots & cov(e_2e_n) & cov(e_2e_{n+1}) & \ldots & cov(e_2e_{n+d}) \\ \vdots & \vdots & \ldots & \vdots & \vdots & \vdots & \vdots \\ cov(e_{n+d}e_1) & cov(e_{n+d}e_2) & \ldots & cov(e_{n+d}e_n) & cov(e_{n+d}e_{n+1}) & \ldots & var(e_{n+d}e_{n+d}) \end{bmatrix} \tag{14}$$

3. Numerical Camera Calibration Example with EW-WTLS Method

This section explains the solution of the camera calibration problem with EW-WTLS method step by step with a real calibration experiment. All necessary data and explanations are given enough to reproduce the experiment.

3.1 Specifications of the Experimental Set-Up and Data Acquisition

In this experiment, Nikon Coolpix L1 digital camera was calibrated. The technical specifications of the camera required for the calibration are as follows: Image sensor type is high density CCD and its dimensions are given as 1/2.5″ (inches) or in millimeters (5.744 mm × 4.308 mm). Focal length of the camera varies between 6.3-31.4 mm. The effective pixels are 6.2 megapixels. Four images were taken with the camera for calibration (Fig. 1). During the acquisition of the images, the camera was rotated approximately 100 gons about the Z axis before the next image had been taken and thus the possible correlations between image geometries are expected to be minimized. The images shown in Fig. 1 are not in their original sizes. The effective dimensions of these four images in pixels are all the same and (2816×2112) pixel^2, where the numbers between parentheses represent width and height of the images respectively. According to the sensor dimensions and the effective pixel area, size of the each detector element of the sensor is obtained as 0.002 mm (2 microns). It is assumed that the detector elements are square and have the same size along the horizontal

and vertical directions. But however, these assumptions were relaxed by adding unknown affine parameters into the calibration model. These two parameters can capture the aspect ratio of the detectors if exists together with the distortions caused by the inevitable errors arose during the mounting of the sensor to the optical system of the camera, as explained in section 2.

As seen in Fig. 1, signalized control points were designed in the scene before image acquisition. 52 control points and 16 tie points were used for the calibration. Object coordinates of 52 control points are given in Tab. A.1 in the appendix A. The object coordinates were measured with a calliper which has ± 10 microns distance measurement precision. In spite of the calliper precision, the resolution of the printer as well as the precision of the human eye which causes some inevitable random errors during the attachment of the printed papers on to the calibration object has been taken into account for computing the precisions of the object coordinates of the signalized points. The points on the above plane between the numbers 1-16 have different precisions from the points on the lower plane. The computed standard deviations used for denoting the precisions for the points 1-16 were obtained as $\sigma_X = \pm 0.102$ mm, $\sigma_Y = \pm 0.102$ mm, and $\sigma_Z = \pm 0.121$ mm for the X, Y, Z coordinates of the points respectively. The precisions of the points on the lower plane were obtained as $\sigma_X = \pm 0.100$ mm $\sigma_Y = \pm 0.100$ mm, and $\sigma_Z = \pm 0.115$ mm. In order to compute those standard deviations, law of the propagation of variances was used.

Image coordinates of the control points were measured from the four images with adaptive least squares matching method [32]. This matching algorithm was implemented in C# by the author for image coordinate measurement tasks. All of the image coordinates have approximately the same precisions which are $\sigma_\xi = \sigma_\eta = \pm 0.0005$ mm for all image points. The origin of the image coordinate system is the center point of each image and the pixel coordinates of the image points were transformed to image coordinate system and thus their metric values were obtained by using the detector size (namely the pixel size, 2 microns). For the details of above procedures, reader is referred to [31]. The measured image coordinates of the control points from three images are given in Table B.1 in the Appendix B.

3.2. Computation of Initial Approximations of Unknowns

Initial approximations of intrinsic parameters are determined from the camera specifications. The most important parameter is the camera constant c. The images given in Fig. 1 were taken with approximately 6.3 mm focal length (with minimum zoom state). So its approximate value was assumed c^0=6.30 mm. The other nine intrinsic parameters were assumed to be zero as initial, because they are strongly expected to be close to zero. Approximate values of the 24 extrinsic parameters should be found by using a closed form or linear solution technique. For this purpose direct linear transformation (DLT) [33] were used and the DLT parameters were estimated with LS. But one may also use another closed form space resection solution method such as given by [34]. The computed initial approximate values are given in Tab. 1.

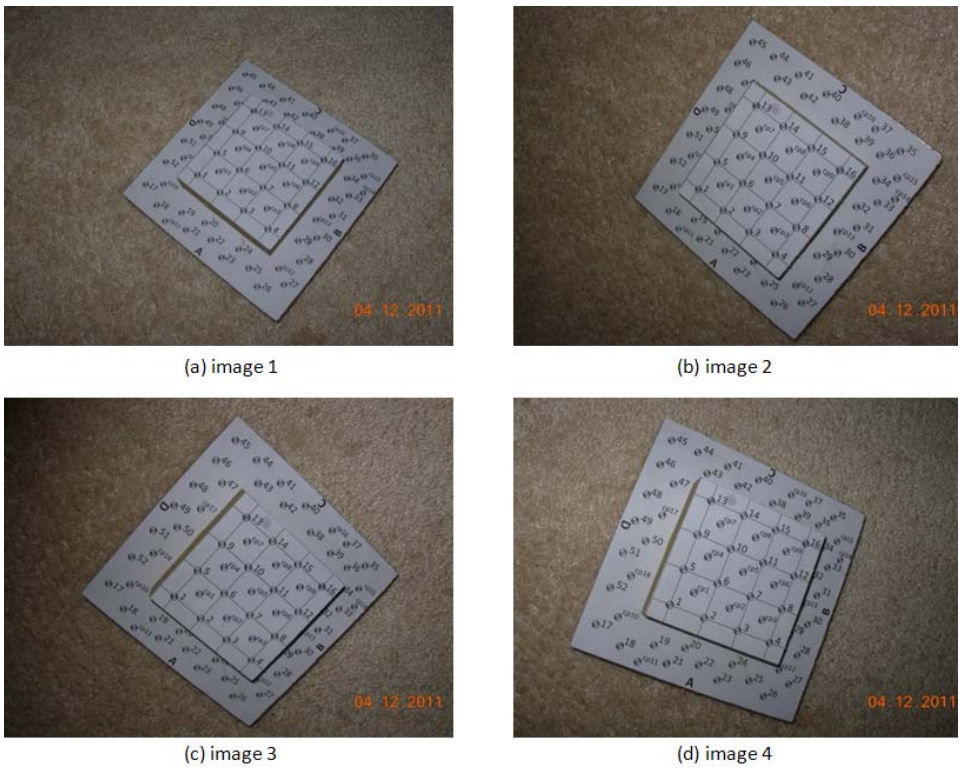

Fig. 1. The images used for calibration.

Tab. 1. Initial approximate values of the unknowns obtained by DLT.

Intrinsic parameters	Extrinsic parameters	Image 1	Image 2	Image 3	Image 4
$c^0 = 6.30$ mm.	ω^0	14.2366 grad	-16.0046 grad	-8.4019 grad	9.1773 grad
$\xi_0^0 = 0.00$ mm.	φ^0	19.7647 grad	17.7970 grad	-12.2905 grad	-15.4562 grad
$\eta_0^0 = 0.00$ mm.	κ^0	41.2861 grad	43.8048 grad	45.7781 grad	25.6221 grad
$k_1^0 = 0.00$	X_0^0	152.7723 mm.	131.4951 mm.	-8.0792 mm.	-2.6024 mm.
$k_2^0 = 0.00$	Y_0^0	-19.4619 mm.	132.7840 mm.	108.2274 mm.	35.8080 mm.
$k_3^0 = 0.00$	Z_0^0	331.9372 mm.	291.6715 mm.	292.8584 mm.	283.7723 mm.
$P_1^0 = 0.00$					
$P_2^0 = 0.00$					
$b_1^0 = 0.00$					
$b_2^0 = 0.00$					

3.3. Computation of Covariance and Weight Matrices of the Rows of the Data Matrix

In the calibration problem, the rows of the data matrix $\mathbf{D} = [\mathbf{A}\ \mathbf{B}]$ are independent from each other and they have different error distributions with different variances. On the other side, the elements of any row are also independent from each other and the covariance matrices of each row are diagonal. If the variances of the elements are known, then the relative weight factors can easily be computed by using those variance values. If the variance of any element is large, this means that this element is more erroneous than the elements with smaller variances, so its weight must be less relative to others.

EW-WTLS estimation results are very sensitive to the weights of the data. For this reason, the weights should be computed in a precise and realistic manner. In general, the precisions of the observed data are known from the measurement model and the used measurement instruments. For example in this calibration experiment, measured quantities are the image coordinates of the control and the tie points and the object coordinates of the control points. Their precisions have been obtained as given in previous section. But when considering the data matrix $\mathbf{D} = [\mathbf{A}\ \mathbf{B}]$it is seen that its sub-matrix $\mathbf{A}$ is of the form equation (13), and $\mathbf{B}$ is equal to the observation vector $\mathbf{b}$. It is clear that the elements of $\mathbf{A}$ are not directly observations themselves, neither image nor object coordinates are they. Those elements are functions of the one or more measurements. So, variance of an individual element of the matrix $\mathbf{A}$ must be affected by the measurement errors. If this element is a function of only one measurement, then its variance is affected by that measurement. But in many cases, an individual element is a function of more than one measurement. This is the case in the calibration problem. In order to find the variances of the matrix elements, the law of propagation of the variances may be used. But if the elements in a row are correlated to each other, then in most cases it is not possible to find the realistic covariances between them. In this paper, the elements in the same row are assumed to be un-correlated. This assumption is reasonable, because the elements of the matrix $\mathbf{A}$ given by the equations (13) are mathematically independent. The variances of the elements of the matrix $\mathbf{A}$ were computed by using the law of the propagation of variances. In this case, the partial derivatives of the matrix elements with respect to the measurements should be computed. These derivatives are too complex and have lengthy formal representations. For computation of the partial derivatives, the vxMaxima 11.04 software was used. vxMaxima is a strong computer algebra software written in LISP and can perform a lot of symbolic mathematical operations including derivatives. Partial derivatives of the matrix elements with respect to the unknown parameters were also computed and added into the variance propagation formula in the calibration program written by the author in C#. If there is no prior information about precisions of these unknowns, their partial derivatives are set to zero and thus not affect the resulting variance. On the other side, if one performs an LS estimation before EW-WTLS, then the a-posteriori precisions of the unknowns obtained from LS may be used to compute the weight information. Especially when there is no prior information this approach may be used. Variances of the vector $\mathbf{b}$ of the data matrix $\mathbf{D}$ are known since they are variances of the measured image coordinates. After all of the variance-covariance matrices of the each row of the data matrix had been computed, proper weights were taken as the reciprocals of the variances.

Figure 2 shows the general flow of the EW-WTLS computations. As seen in Fig. 2, there are two separate iteration loops. One is for the non linear solution of EW-WTLS, and the one for controlling the convergence of the non-linear bundle adjustment procedure. If the bundle adjustment does not converge to the solution by the means of convergence criterions, then both the data $\mathbf{D}$ and weight matrices are updated with the results of the current iteration and the next iteration steps continue with the updated data. The details of the EW-WTLS iterations shown in the figure may be found in [9] and its MATLAB® implementation in [35].

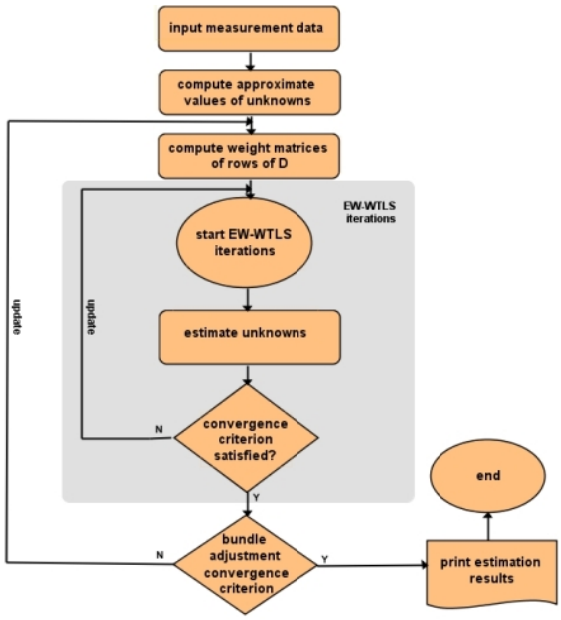

Fig. 2. Camera calibration process with EW-WTLS bundle adjustment.

The estimated final results of the calibration parameters are given in Tab. 2 for EW-WTLS and in Tab. 3 for LS. The standard deviation of the data with unit weight was also computed for both methods.

Tab. 2. Estimation results of the calibration parameters with EW-WTLS.

Intrinsic parameters	Extrinsic parameters	Image 1	Image 2	Image 3	Image 4
= 6.32163324 mm.		14.20606 grad	-16.00527 grad	-8.40233 grad	9.14045 grad
-0.09544115 mm.		19.64449 grad	17.67369 grad	-12.40555 grad	-15.54941 grad
0.052469424 mm.		41.29834 grad	43.79702 grad	45.76343 grad	25.60859 grad
-0.00833065		152.7721 mm.	131.4947 mm.	-8.0794 mm.	-2.6024 mm.
0.00059490		-19.4621 mm.	132.7838 mm.	108.2274 mm.	35.8081 mm.
-0.00004849		331.9373 mm.	291.6711 mm.	292.8586 mm.	283.7724 mm.
-0.00111310					
0.00057805					
0.00481168					
0.00007652					
0.00002 mm.					

Tab. 3. Estimation results of the calibration parameters with LS.

Intrinsic parameters	Extrinsic parameters	Image 1	Image 2	Image 3	Image 4
6.32618224 mm.		14.25810 grad	-15.95911 grad	-8.36024 grad	9.20014 grad
-0.09542377 mm.		19.68993 grad	17.71349 grad	-12.36548 grad	-15.52731 grad
0.05839393 mm.		41.28505 grad	43.78825 grad	45.77478 grad	25.62382 grad
-0.00833139		152.8885 mm.	131.5581 mm.	-8.1188 mm.	-2.6590 mm.
0.00057688		-19.5146 mm.	132.8456 mm.	108.2739 mm.	35.7734 mm.
-0.00004084		332.1410 mm.	291.8701 mm.	293.0555 mm.	283.9613 mm.
-0.00109668					
0.00064189					
0.00482266					
0.00002534					
0.04210 mm.					

3.4. Comparison of EW-WTLS and LS Calibration Results

In order to compare the estimation results given in Table 2 and Table 3, some comparison measures are required. As seen in Table 2 and Table 3, the estimation results of EW-WTLS and LS are slightly different. The standard deviations of the data with unit weights are 0.00002 mm. for EW-WTLS and 0.04210 mm. for LS estimations respectively. According to these standard deviations, it seems that EW-WTLS results are more precise. The estimated intrinsic parameter values are almost the same for two methods, but the extrinsic parameter values are slightly different. The maximum difference between projection centre coordinates is 203 microns, and the maximum difference between rotation angles is $5^c\ 97^{cc}$ (0.0597 grad). When these maximum differences are considered it is seen that they are reasonable. In order to see the effects

of the differences of the parameter values on the object coordinates, check points may be used. In this experiment, the object coordinates of the check points have been estimated within the bundle adjustment model. For this purpose, check points were assumed to be tie points in the model and so their object coordinates are unknowns of the bundle adjustment. The bundle adjustment calibration model was solved both with EW-WTLS and LS separately. Computed object coordinates of the check points have been compared to the actual known coordinates. The more precise and accurate parameters set should give the closer coordinate values to the actual known coordinates. In the Table C.1 and Table C.2 in the appendix C, the known check point coordinates and their measured image coordinates used in this experiment have respectively been given. Each check point has eight image coordinates which have been measured from four images. In Table 4, computed check point coordinates from EW-WTLS and LS estimations were given. The differences of the estimated coordinate values from the actual known coordinates were also given in the table.

Tab. 4. Comparison of the actual object coordinates of the check points estimated with EW-WTLS and LS bundle adjustment given in Tab. 2. and 3.

Point #	EW-WTLS results						Point #	LS results					
	X [mm]	Y [mm]	Z [mm]	ΔX [mm]	ΔY [mm]	ΔZ [mm]		X [mm]	Y [mm]	Z [mm]	ΔX [mm]	ΔY [mm]	ΔZ [mm]
cp 1	50.0209	51.5192	18.8721	-0.1029	0.1448	0.1279	cp 1	50.0174	51.5200	18.8733	-0.0994	0.1440	0.1267
cp 2	71.4286	50.9307	18.7443	-0.0846	0.0193	0.2557	cp 2	71.4285	50.9327	18.7447	-0.0845	0.0173	0.2553
cp 3	91.3707	51.4939	18.7666	-0.1247	-0.1119	0.2334	cp 3	91.3722	51.4888	18.7661	-0.1262	-0.1068	0.2339
cp 4	50.0467	72.0581	18.9478	-0.0447	0.0599	0.0522	cp 4	50.0382	72.0606	18.9497	-0.0362	0.0574	0.0503
cp 5	71.3366	71.9795	18.7389	0.0074	-0.0615	0.2611	cp 5	71.3288	71.9902	18.7400	0.0152	-0.0722	0.2600
cp 6	90.7941	72.0651	18.9451	0.0189	-0.1471	0.0549	cp 6	90.8033	72.0994	18.9410	0.0097	-0.1814	0.0590
cp 7	49.8326	91.2211	18.9167	0.0854	0.0829	0.0833	cp 7	49.8624	91.2094	18.9187	0.0556	0.0946	0.0813
cp 8	71.0737	92.4878	18.7860	0.0543	-0.0338	0.2140	cp 8	71.0298	92.4804	18.7858	0.0982	-0.0264	0.2142
cp 9	90.7804	92.3881	18.8247	0.0326	-0.1501	0.1753	cp 9	90.7347	92.3749	18.8191	0.0783	-0.1369	0.1809
cp10	18.8676	24.2545	-0.1763	-0.0346	-0.1035	0.1763	cp10	18.8516	24.1953	-0.1509	-0.0186	-0.0443	0.1509
cp11	38.1458	4.8180	-0.2093	-0.0118	0.0460	0.2093	cp11	38.1514	4.8211	-0.2005	-0.0174	0.0429	0.2005
cp14	133.4443	105.4459	0.3574	-0.1213	0.0201	-0.3574	cp14	133.4188	105.4353	0.3822	-0.0958	0.0307	-0.3822
cp15	127.0773	115.5214	0.4221	-0.1143	0.0276	-0.4221	cp15	127.0546	115.4912	0.4477	-0.0916	0.0578	-0.4477
cp16	87.9496	129.7059	0.1856	-0.0276	0.0891	-0.1856	cp16	87.9401	129.6702	0.1800	-0.0181	0.1248	-0.1800
cp17	20.5715	86.2776	0.3949	0.0155	-0.0986	-0.3949	cp17	20.5428	86.1658	0.3993	0.0442	0.0132	-0.3993
cp18	17.2094	47.9923	0.0421	0.0876	0.0497	-0.0421	cp18	17.2093	47.9948	0.0449	0.0877	0.0472	-0.0449

For the comparison of the results the empirical precisions may be used. The average empirical precisions give the real accuracy of the estimated coordinates [31]. The empirical precisions are computed from the differences between the known (Tab. C.1) and the computed (Tab. 4) coordinates of the check points as follows.

$$\bar{\mu}_X = \sqrt{\frac{\sum \Delta X_i^2}{n_X}} \quad \bar{\mu}_Y = \sqrt{\frac{\sum \Delta Y_i^2}{n_Y}} \quad \bar{\mu}_{XY} = \sqrt{\frac{\bar{\mu}_X{}^2 + \bar{\mu}_Y{}^2}{2}} \quad \bar{\mu}_Z = \sqrt{\frac{\sum \Delta Z_i^2}{n_Z}} \tag{16}$$

where, ΔX_i, $\Delta Y_i, \Delta Z_i$ are the coordinate differences between the known and the estimated coordinates. n_X, n_Y, n_Z are the number of the check point coordinates in X, Y and Z respectively. The average empirical precisions obtained from the Equation (16) are $\bar{\mu}_{X_{LS}} = \pm 0.07143$ mm., $\bar{\mu}_{Y_{LS}} = \pm 0.08955$ mm., $\bar{\mu}_{XY_{LS}} = 0.08100$ mm., and $\bar{\mu}_{Z_{LS}} = \pm 0.23692$ mm. The average precisions obtained from the EW-WTLS estimation are $\bar{\mu}_{X_{EW-WTLS}} = \pm 0.07281$ mm., $\bar{\mu}_{Y_{EW-WTLS}} = \pm 0.08928$ mm., $\bar{\mu}_{XY_{EW-WTLS}} = \pm 0.08146$ mm., and $\bar{\mu}_{Z_{EW-WTLS}} = \pm 0.23271$ mm. As seen the empirical precision of the EW-WTLS and LS estimations are almost equal to each other.

Now a question comes: "Which of the estimated parameter sets is more precise and more accurate?" As seen from the results, the answer is clear. One may use either of them. Then really, such a question seems unnecessary as discussed by [4, 25]. But however, as stated in the previous sections, from the theoretical point of view EW-WTLS or generally the eiv models are more realistic, one may prefer to use the estimated parameter set from EW-WTLS. But when the computation complexity and numerical stability problems of the EW-WTLS are considered, another one may prefer the LS estimation. Both preferences are suitable as seen in this experimental test.

Finally, for the visual evaluation tasks, camera distortion vectors obtained with EW-WTLS and LS estimation methods have been given in the Figures 3 and 4 respectively. X and Y axes of the figures represent the pixel coordinate system of an image taken with the calibrated camera. The vectors in the figures represent the total distortions at the vector locations and their lengths are proportional to their magnitudes. The directions of the arrows show the directions of changes of the image coordinates due to the distortion effects. The scales of the both visual graphics in the figures are the same. The minimum and maximum values of the total x (ξ) components of the distortion vectors of EW-WTLS are $\min\{dx = d\xi\} = -0.395$ mm and $\max\{dx = d\xi\} = 0.260$ mm. The minimum and maximum values of the total y (η) components are $\min\{dy = d\eta\} =$

-0.226 mm and $\max\{dy = d\eta\} = 0.280$ mm. According to these values minimum and maximum total distortion magnitudes obtained by EW-WTLS are $\min\{dist\} = 0.0$ and $\max\{dist\} = 0.485$ mm.

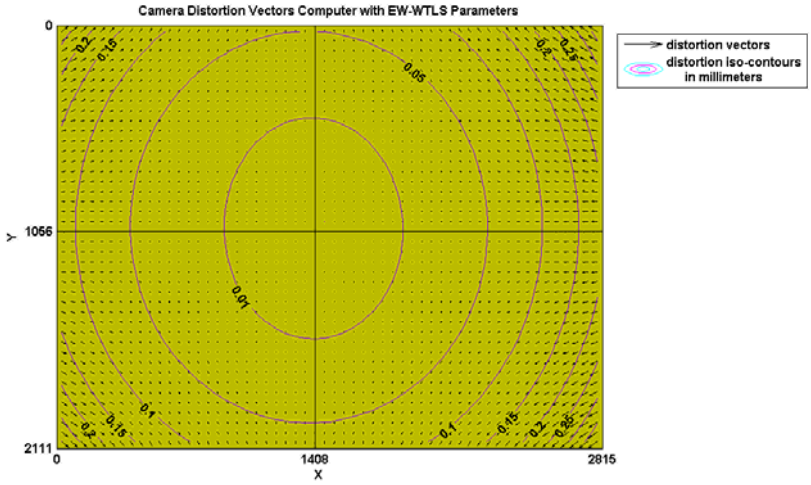

Fig. 3. Distortion vectors after EW-WTLS bundle adjustment.

The minimum and maximum values of the total x (ξ) components of the distortion vectors of LS are $\min\{dx = d\xi\} = -0.355$ mm and $\max\{dx = d\xi\} = 0.232$ mm. The minimum and maximum values of the total y (η) components are $\min\{dy = d\eta\} = -0.197$ mm and $\max\{dy = d\eta\} = 0.252$ mm. According to these values minimum and maximum total distortion magnitudes obtained by LS are $\min\{dist\} = 0.0$ and $\max\{dist\} = 0.436$ mm.

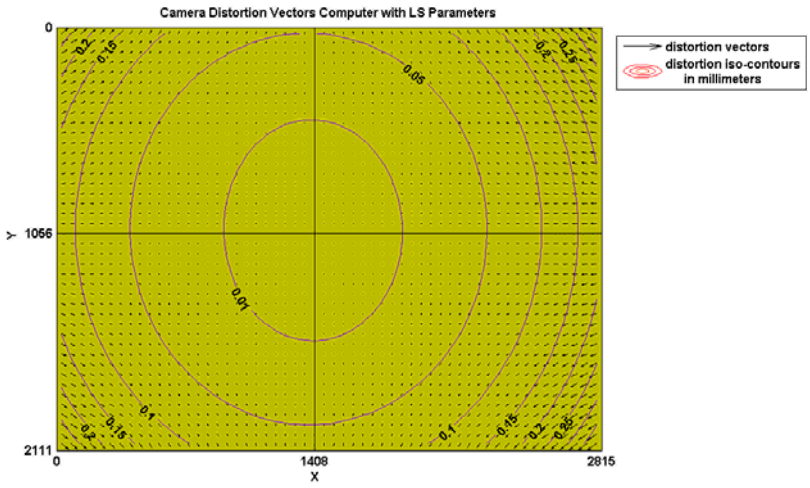

Fig. 4. Distortion vectors after LS bundle adjustment.

As seen in the figures, magnitudes of the maximum distortion values obtained from the EW-WTLS are greater than the maximum distortion values of the LS. But since the maximum distortions are located at the corner regions of the images, for the rest of the image areas the distortion magnitudes obtained from EW-WTLS and LS are almost the same.

4. Conclusions

In this paper it has been shown that the EW-WTLS estimation method gives almost the same precision and accuracy as LS for the camera calibration problem. In the most of the papers in the literature on the variants of the TLS and the errors in variables models, it is claimed that those models give more precise and accurate results than LS. These claims essentially originate from the statistically more improved theoretical model of the TLS estimation methods. Because, in the normal situations, improvements in the theoretical basis of any model causes one to expect better practical results from this model. This is of course the case must be true for ideal situations. But however, there are numerous unexpected factors that may influence and take away the ideal expectations from the desired practical results. In this present work, it has been seen that the both EW-WTLS and LS methods have given almost the same results by the means of the precision and accuracy, although

EW-WTLS has a statistically more realistic model. This situation mainly arises from the fact that even the ideal theory of the EW-WTLS is stronger than LS, in practice the statistical definition of the behavior of the errors in the data matrix cannot in general be realistic. On the other side, the calibration experiment has showed that the EW-WTLS solution is very sensitive to the weights of the data. Note that the weights are computed from the data statistics and so in this case, if the covariance information of the data are not at hand apriori or cannot be estimated properly, then this kind of imprecise covariance information cause the theoretical model to be deviated from the actual real case. It is not also possible and there is no way to define the exact real statistical relations between the data elements. So it is unnecessary and useless job to discuss whether TLS or its variants and LS methods are more precise and accurate. This means that one may of course prefer one method or the other. Either of them is acceptable as shown in the paper. But however, if it is believed that the apriori statistical information of the data are known in a precise manner, than choosing the TLS variants (or errors in variables models) might be more reasonable, since its statistical model is theoretically more realistic and since the apriori information are believed to be close enough to the unknown reality. As a final remark, it may be said that the more realistic theoretical model does not mean more precise and more accurate practical results.

Appendix A.

Tab. A.1. Object coordinates of the control points.

Point #	X [mm]	Y [mm]	Z [mm]	Point #	X [mm]	Y [mm]	Z [mm]	Point #	X [mm]	Y [mm]	Z [mm]
1	40.063	41.000	19.000	18	25.632	9.686	0.000	35	119.286	128.699	0.000
2	60.063	41.000	19.000	19	43.398	16.699	0.000	36	111.390	119.932	0.000
3	80.064	41.000	19.000	20	60.725	21.302	0.000	37	100.424	130.014	0.000
4	100.062	41.000	19.000	21	53.926	9.467	0.000	38	78.710	119.932	0.000
5	40.188	61.000	19.000	22	71.691	14.946	0.000	39	96.914	119.056	0.000
6	60.188	61.000	19.000	23	85.290	10.343	0.000	40	65.331	129.357	0.000
7	80.189	61.000	19.000	24	90.554	21.741	0.000	41	44.933	128.699	0.000
8	100.187	61.000	19.000	25	103.933	16.042	0.000	42	55.022	120.590	0.000
9	40.313	81.000	19.000	26	116.216	10.124	0.000	43	35.283	119.494	0.000
10	60.313	81.000	19.000	27	128.937	21.960	0.000	44	25.413	128.699	0.000
11	80.314	81.000	19.000	28	127.621	40.371	0.000	45	8.744	128.699	0.000
12	100.312	81.000	19.000	29	118.409	51.110	0.000	46	8.305	112.699	0.000
13	40.438	101.000	19.000	30	126.963	60.316	0.000	47	19.710	105.466	0.000
14	60.438	101.000	19.000	31	126.305	78.946	0.000	48	8.086	93.631	0.000
15	80.439	101.000	19.000	32	118.628	88.371	0.000	49	7.647	77.412	0.000
16	100.437	101.000	19.000	33	126.743	97.795	0.000	50	17.517	69.083	0.000
17	8.963	16.042	0.000	34	118.409	107.220	0.000	51	8.305	58.343	0.000
								52	8.963	37.740	0.000

Appendix B.

Tab. B.1. Image coordinates of the control points.

Point #	Image 1 [mm]		Image 2 [mm]		Image 3 [mm]		Image 4 [mm]		Point #	Image 1 [mm]		Image 2 [mm]		Image 3 [mm]		Image 4 [mm]		Point #	Image 1 [mm]		Image 2 [mm]		Image 3 [mm]		Image 4 [mm]	
	ξ	η	ξ	η	ξ	η	ξ	η		ξ	η	ξ	η	ξ	η	ξ	η		ξ	η	ξ	η	ξ	η	ξ	η
1	-0.3673	0.0138	-0.5218	-0.1704	-0.6552	-0.3611	-0.8738	-0.4613	22	-0.2013	-0.7937	-0.1920	-0.9337	-0.5112	-1.0197	-0.5202	-1.2099	43	0.4731	0.9273	0.4568	1.1976	0.3865	1.0436	-0.4118	1.1701
2	-0.0833	-0.2057	-0.2126	-0.4329	-0.3268	-0.6325	-0.4488	-0.6263	23	-0.0653	-1.0157	-0.0451	-1.1789	-0.3702	-1.2447	-0.2889	-1.3976	44	0.4396	1.1197	0.4117	1.4674	0.3684	1.3337	-0.5273	1.4289
3	0.2085	-0.4292	0.1063	-0.7032	-0.0064	-0.8959	-0.0357	-0.7853	24	0.1449	-0.9101	0.1629	-1.0767	-0.1431	-1.1493	-0.1027	-1.2038	45	0.2265	1.2594	0.1534	1.6499	0.1047	1.5814	-0.8523	1.5833
4	0.5094	-0.6591	0.4336	-0.9797	0.3035	-1.1486	0.3590	-0.9343	25	0.2688	-1.1459	0.2992	-1.3352	-0.0241	-1.3810	0.1032	-1.4067	46	0.0571	1.0870	-0.0363	1.3895	-0.1354	1.3323	-0.9953	1.2790
5	-0.1259	0.2856	-0.2901	0.1643	-0.3635	-0.0375	-0.7034	-0.0238	26	0.3781	-1.3764	0.4153	-1.5838	0.0722	-1.5956	0.2855	-1.6005	47	0.1250	0.9010	0.0541	1.1408	-0.0590	1.0479	-0.8269	1.0384
6	0.1562	0.0757	0.0281	-0.0968	-0.0350	-0.3191	-0.2824	-0.1933	27	0.7084	-1.3510	0.7563	-1.5793	0.4036	-1.5808	0.5982	-1.4491	48	-0.1494	0.8664	-0.2516	1.0773	-0.4177	1.0281	-1.1612	0.9078
7	0.4495	-0.1426	0.3566	-0.3662	0.2861	-0.5905	0.1249	-0.3614	28	0.9009	-1.0663	0.9642	-1.2863	0.6268	-1.3234	0.7046	-1.0902	49	-0.3310	0.6768	-0.4353	0.8184	-0.6548	0.7738	-1.3081	0.5853
8	0.7504	-0.3646	0.6933	-0.6421	0.5915	-0.8522	0.5144	-0.5179	29	0.8869	-0.8052	0.9495	-0.9957	-	-	-	-	50	-0.2987	0.4849	-0.3863	0.5708	-0.6146	0.5013	-1.1739	0.3294
9	0.1071	0.5508	-0.0505	0.5084	-0.0618	0.2909	-0.5322	0.4101	30	1.1177	-0.7700	1.2078	-0.9642	0.8855	-1.0464	0.8320	-0.7056	51	-0.5348	0.4389	-0.6310	0.5061	-0.9160	0.4621	-1.4554	0.1867
10	0.3908	0.3486	0.2773	0.2506	0.2666	0.0017	-0.1180	0.2329	31	1.3118	-0.4994	1.4411	-0.6493	1.1300	-0.7762	0.9477	-0.3478	52	-0.7583	0.1728	-0.8339	0.1779	-1.1845	0.1309	-1.6160	-0.2478
11	0.6834	0.1384	0.6154	-0.0165	0.5827	-0.2781	0.2812	0.0579	32	1.2989	-0.2880	1.4358	-0.3889	-	-	-	-									
12	0.9817	-0.0766	0.9614	-0.2951	0.8852	-0.5461	0.6654	-0.1071	33	1.5169	-0.2453	1.6985	-0.3390	1.3924	-0.5173	1.0800	-0.0011									
13	0.3350	0.8075	0.1967	0.8626	0.2430	0.6254	-0.3618	0.8294	34	1.4934	-0.0302	1.6838	-0.0619	-	-	-	-									
14	0.6177	0.6123	0.5322	0.6056	0.5694	0.3272	0.0445	0.6478	35	1.7211	0.2397	1.9855	0.2981	1.7190	0.0241	1.1535	0.6204									
15	0.9079	0.4101	0.8800	0.3393	0.8831	0.0395	0.4361	0.4691	36	1.5213	0.2059	1.7305	0.2504	1.4938	-0.0001	0.9663	0.5265									
16	1.2055	0.2011	1.2349	0.0652	1.1819	-0.2342	0.8114	0.2987	37	1.4664	0.4429	1.6725	0.5713	1.4850	0.2921	0.8467	0.7990									
17	-1.0082	-0.1047	-1.0469	-0.1478	-1.4711	-0.1996	-1.7954	-0.7036	38	1.0615	0.5282	1.1723	0.6760	1.0395	0.4365	0.3989	0.7992									
18	-0.8729	-0.3620	-0.8891	-0.4400	-1.2866	-0.5141	-1.4955	-0.9730	39	1.3091	0.3408	1.4697	0.4264	1.2862	0.1755	0.7153	0.6310									
19	-0.5612	-0.4574	-0.5754	-0.5521	-0.9207	-0.6413	-1.0725	-0.9639	40	0.9733	0.7666	1.0665	1.0064	0.9788	0.7680	0.2247	1.0868									
20	-0.2760	-0.5831	-0.2817	-0.6998	-0.5943	-0.7926	-0.6858	-1.0003	41	0.6929	0.9472	0.7225	1.2414	0.6685	1.0496	-0.1562	1.2548									
21	-0.5083	-0.6709	-0.5058	-0.7906	-0.8537	-0.8766	-0.9172	-1.1926	42	0.7452	0.7594	0.7872	0.9814	0.7027	0.7784	-0.0299	1.0157									

Note: *The points with the numbers 29, 32 and 34 are invisible in the images 3 and 4.*

Appendix C.

Tab. C.1. Known object coordinates of the check points.

Point #	X [mm]	Y [mm]	Z [mm]	Point #	X [mm]	Y [mm]	Z [mm]
cp1	49.9180	51.6640	19.0000	cp 9	90.8130	92.2380	19.0000
cp2	71.3440	50.9500	19.0000	cp10	18.8330	24.1510	0.0000
cp3	91.2460	51.3820	19.0000	cp11	38.1340	4.8640	0.0000
cp4	50.0020	72.1180	19.0000	cp14	133.3230	105.4660	0.0000
cp5	71.3440	71.9180	19.0000	cp15	126.9630	115.5490	0.0000
cp6	90.8130	71.9180	19.0000	cp16	87.9220	129.7950	0.0000
cp7	49.9180	91.3040	19.0000	cp17	20.5870	86.1790	0.0000
cp8	71.1280	92.4540	19.0000	cp18	17.2970	48.0420	0.0000

Tab. C.2. Image coordinates of the check points.

Point #	Image 1 [mm]		Image 2 [mm]		Image 3 [mm]		Image 4 [mm]	
	ξ	η	ξ	η	ξ	η	ξ	η
cp 1	-0.1014	0.0562	-0.2486	0.3393	-0.3270	-0.1220	-0.5771	-0.3099
cp 2	0.1991	-0.1881	0.0858	-0.0005	-0.6279	-0.4182	-0.1355	-0.5037
cp 3	0.5012	-0.4046	0.4198	0.3185	-0.8823	-0.6830	0.2669	-0.6512
cp 4	0.1413	0.3357	-0.0019	-0.0344	0.0032	0.2293	-0.4019	0.1337
cp 5	0.4471	0.1075	0.3477	0.3075	-0.2978	-0.0554	0.0330	-0.0546
cp 6	0.7363	-0.1008	0.6776	0.6101	-0.5627	-0.3218	0.4174	-0.2161
cp 7	0.3584	0.5905	0.2317	0.2528	0.3211	0.5674	-0.2473	0.5404
cp 8	0.6774	0.3895	0.6046	0.6086	0.0350	0.3105	0.1890	0.3759
cp 9	0.9662	0.1817	0.9447	0.9087	-0.2433	0.0380	0.5674	0.2018
cp10	-0.7907	-0.1012	-0.8362	-1.2065	-0.2098	-0.1441	-1.5200	-0.6142
cp11	-0.7697	-0.5627	-0.7685	-1.1563	-0.7447	-0.6611	-1.2752	-1.1698
cp14	1.6930	-0.2107	1.9172	1.5853	-0.4885	-0.2969	1.2388	0.0912
cp15	1.7018	-0.0094	1.9429	1.6411	-0.2660	-0.0369	1.1986	0.3244
cp16	1.2878	0.5599	1.4545	1.3088	0.4577	0.7293	0.6301	0.9005
cp17	-0.0709	0.6677	-0.1539	-0.3245	0.7269	0.8127	-0.9689	0.6493
cp18	-0.5382	0.2226	-0.6150	-0.9126	0.1740	0.23970	-1.3565	-0.1040

The author declares that there is no conflict of interests regarding the publication of this article.

References

[1] Gruen A, Beyer HA (eds.): System calibration through self-calibration., *1st edn. Berlin, Germany: Springer Verlag; 2001.*

[2] Weng J, Cohen P, Herniou M: Camera calibration with distortion models and accuracy evaluation. *IEEE Transactions on Pattern Analysis and Machine Intelligence 1992, 14(10):965-980.*

[3] Kraus K: Photogrammetry, *Advanced Methods and Applications, vol. 2, 4th edn. Bonn, Germany: Dümmlers Verlag; 1997.*

[4] Neitzel F: Generalization of total least-squares on example of unweighted and weighted 2D similarity transformation. *Journal of Geodesy 2010, 84(12):751-762.*

[5] Grafarend EW: Linear and nonlinear models: Fixed Effects, *Random Effects, and Mixed Models. Berlin: Walter de Gruyter GmbH & Co. Kg.; 2006.*

[6] Golub GH, Loan CFV: An analysis of the total least squares problem. *SIAM Journal of Numerical Analysis 1980, 17:883-893.*

[7] Huffel SV, Vandewalle J: The Total Least Squares Problem: Computational Aspects and Analysis, *1st edn. Philadelphia, USA: SIAM; 1991.*

[8] Markovsky I, van Huffel S: Overview of total least squares methods. *Signal Processing 2007, 87(10):2283-2302.*

[9] Markovsky I, Rastello ML, Premoli A, Kukush A, Van Huffel S: The element-wise weighted total least-squares problem *Computational Statistics and Data Analysis 2006, 50:181-209.*

[10] Rastello ML, Premoli A: Least squares problems with element-wise weighting. *Metrologia 2006, 43:260-267.*

[11] Van Huffel S, Vandewalle J: Analysis and properties of the generalized total least squares problem AX»B when some or all columns in A are subject to error. *SIAM J Matrix Anal Appl 1989, 10(3):294-315.*

[12] Mühlich M, Mester R: A considerable improvement in non-iterative homography estimation using TLS and equilibration. *Pattern Recognition Letters 2001, 22(11):1181-1189.*

[13] Mühlich M, Mester R: Subspace Methods and Equilibration in Computer Vision. *In: Scandinavian Conference on Image Analysis: 2001; Bergen, Norway.*
[14] Demmel JW: The smallest perturbation of a submatrix which lowers the rank and constrained total least squares problems. *SIAM Journal of Numerical Analysis 1987, 24(1):199-206*.
[15] Golub GH, Hoffman A, Stewart GW: A generalization of the Eckart-Young-Mirsky Matrix Approximation Theorem. *Linear Algebra and Its Applications 1987, 88-89:317-327*.
[16] Wei M, Zhang J: On perturbations of some constrained subspaces. *Journal of Computational and Applied Mathematics 2009, 226:155-165*.
[17] Nayak A, Trucco E, Thacker NA: Comparing the performance of least-squares estimators: when is GTLS better than LS? In: Technical Report Tina Memo No 2005-011. *Imaging Science and Biomedical Engineering Division, Medical School, University of Manchester.; 2005.*
[18] De Moor B: Structured total least squares and L2 approximation problems. *Linear Algebra and Its Applications 1993, 188-189:163-205*.
[19] Overview of total least squares methods
[20] Krystek M, Anton M: A weighted total least-squares algorithm for fitting a straight line. *Measurement Science and Technology 2007, 18:3438-3442*.
[21] Krystek M, Anton M: A least squares algorithm for fitting data points with mutually correlated coordinates to a straight line. *Measurement Science and Technology 2011, 22:35101-35109*.
[22] Markovsky I, Sima DM, Van Huffel S: Total least squares methods. *Wiley Interdisciplinary Reviews:Computational Statistics 2010, 2(2):212-217*.
[23] Schaffrin B, Felus YA: Multivariate total least-squares adjustment for empirical affine transformations. *In: Series: International Association of Geodesy Symposia. Edited by Xu P, Liu J, Dermanis A, vol. 132. Berlin, Germany: Springer-Verlag; 2008: 238-242*.
[24] Shen Y, Li B, Chen Y: An iterative solution of weighted total least-squares adjustment. *Journal of Geodesy 2011, 85(4):229-238*
[25] Schaffrin B, Lee I, Choi Y, Felus Y: Total Least-Squares (TLS) for geodetic straight-line and plane adjustment. *Bollettino di geodesia e scienze affini 2006. , 65(3):141-168*.
[26] Yi C, Jue L: Performing space resection using total least squares. *The International Archives of the Photogrammetry, Remote Sensing and Spatial Information Sciences 2008, 37.(B3):11-14*.
[27] Dogan S, Altan MO: Total Least Squares Registration of Images for Change Detection. *International Archives of the Photogrammetry, Remote Sensing and Spatial Information Sciences 2010, 38(4-8-2):180-184.*
[28] Brown DC: Close-range camera calibration. *Photogrammetric Engineering and Remote Sensing 1971, 37(8):855-866.*
[29] Remondino F, Fraser C: Digital camera calibration methods: considerations and comparisons. *International Archieves of Photogrammetry and Remote Sensing 2006, 36(5):266-272*.
[30] Bradsky G, Kaehler A: Learning OpenCV computer vision with the OpenCV library. *CA., USA.: O'Reilly Media Inc.; 2008*.
[31] Remondino F: Investigation and Calibration of Sony DSC-F505 Cybershot. *In: Praktikum in Photogrammetry. Zurich, Switzerland.: Institue of Geodesy and Photogrammetry ETH-Hönggerberg; 2000*.
[32] Gruen A: Adaptive least squares correlation: a powerful image matching technique. *South African Journal of Photogrammetry, Remote Sensing and Cartography 1985, 14(3):175-187*.
[33] Abdel-Aziz YI, Karara HM: Direct linear transformation from comparator coordinates into object space coordinates in close-range photogrammetry. *In: Symposium on Close-Range Photogrammetry: 1971; Falls Church, VA.: American Society of Photogrammetry.: 1-18.*
[34] Zeng Z, Wang X: A general solution of a closed form space resection. *Photogrammetric Engineering and Remote Sensing 1992, 58(3):327-338.*
[35] Markovsky I, Van Huffel S: A Matlab toolbox for weighted total least squares approximation. *In: Technical Report 04–220. Leuven-Heverlee, Belgium.: Department of Electrical Engineering, K.U.Leuven.; 2004.*